RSC Advances

PAPER

Cite this: *RSC Adv.*, 2023, **13**, 13725

A controllably fabricated polypyrrole nanorods network by doping a tetra-β-carboxylate cobalt phthalocyanine tetrasodium salt for enhanced ammonia sensing at room temperature†

Shijie Gai,[a] Xiaolin Wang,[b] Runze Zhang,[a] Kun Zeng,[a] Shoulei Miao,[a] Yiqun Wu[ac] and Bin Wang *[a]

The morphology adjustment and functional doping optimization of polypyrrole (PPy) are of great significance in improving its gas sensing performance. Here, the PPy-0.5TcCoPc nanorods with a uniform dispersed 3-D network were prepared using one-step *in situ* polymerization using the electrostatic interaction between dopant counterion substituents in tetra-β-carboxylate cobalt phthalocyanine tetrasodium salt (TcCoPcTs) with larger space structure and pyrrole (Py) molecules, in which TcCoPcTs is not only used as a dopant molecule crosslinking PPy chains to obtain a 3-D network, thus improving the conductivity, but also as a sensor accelerator to improve the gas-sensing performance. The resulting PPy-TcCoPc hybrid exhibits superior NH_3-sensing properties than PPy and tetra-β-carboxylate cobalt phthalocyanine (TcCoPc) under the same test conditions, especially the PPy-0.5TcCoPc sensor shows ultrafast response/recovery time to 50 ppm NH_3 (8.1 s/370.8 s), low detection limit of 8.1 ppb and excellent gas selectivity at room temperature (20 °C). Besides, the PPy-0.5TcCoPc sensor also maintains superior response (49.3% to 50 ppm NH_3), humidity resistance and conspicuous stability over 45 days. The excellent NH_3-sensing performance of the PPy-0.5TcCoPc hybrid arises from the excellent gas selectivity of TcCoPc, the remarkable response mechanism between PPy and NH_3, the high electrical conductivity, abundant active sites and good electron transport ability of the unique 3-D network with large specific surface area. The morphology regulation and functional doping optimization strategy of TcCoPcTs doped PPy broaden the research direction of ideal gas sensor materials.

Received 6th January 2023
Accepted 13th April 2023

DOI: 10.1039/d3ra00103b

rsc.li/rsc-advances

Introduction

Ammonia (NH_3) is a common chemical raw material, which is used in fertilizers, pharmaceuticals, light industry, organic intermediate preparation and many other industrial fields. Meanwhile, it is also produced in livestock waste, industrial and automobile emissions.[1–4] However, NH_3 is a harmful gas, which can cause serious damage to human health when inhaled in large amounts for a short period or when exposed to low concentrations for a long time. It is understood that the NH_3 exposure limit is 25 ppm (TWA).[5,6] Therefore, there is a need for the rapid and efficient detection of NH_3.

Depending on the sensing mechanisms and testing conditions, gas sensors are mainly divided into: semiconductor gas sensors,[7–12] electrochemical gas sensors,[13,14] acoustic sensors[15] and optical sensors.[16–18] Compared with electrochemical sensors, which require electrolytes and noble metal electrodes, and the other two types of gas sensors, which are more cumbersome, semiconductor gas sensors are currently a hot research topic because of their ease of operation, simple preparation and compatibility.[19–21]

As a P-type semiconductor material, conductive polymers not only have a good gas response to NH_3, but also have the ability to work at room temperature. Among them, polypyrrole (PPy) is considered a promising material to detect NH_3 because of its high affinity and low redox potential for reduced NH_3 molecules and pyrrole (Py) main chains,[22] especially fast response speed. However, pristine PPy still has the disadvantages of low sensitivity, weak recovery ability, poor selectivity, and short life due to the disordered aggregation structure, low utilization of Py monomers, which still do not meet the demands of real applications.[23,24] Therefore, it is very important to overcome its own

[a]*Key Laboratory of Functional Inorganic Material Chemistry, Ministry of Education, School of Chemistry and Materials Science, Heilongjiang University, Harbin, 150080, China. E-mail: wangbin@hlju.edu.cn*

[b]*School of Material and Chemical Engineering, Heilongjiang Institute of Technology, Harbin, 150050, P. R. China*

[c]*Shanghai Institute of Optics and Fine Mechanics, Chinese Academy of Sciences, P.O. Box 800216, Shanghai, 201800, China*

† Electronic supplementary information (ESI) available: Other detailed characterization. See DOI: https://doi.org/10.1039/d3ra00103b

shortcomings and improve its conductivity, response, recovery ability and selectivity towards NH_3.

The morphology regulation and functional doping optimization of PPy are effective ways to improve its conductivity and NH_3-sensing.[25–27] It is noteworthy that the morphology and electrical conductivity of PPy can be optimized by chemical doping.[28] Since pyrrole is easily oxidized to the positive radical and deprotonated, common dopants used for PPy are some anions.[29–31] Undoped PPy acts like an insulator, while the doped PPy exhibits shows doped semiconductors with conductivity of more than 100 s m^{-1}.[32] Therefore, suitable doping of PPy may facilitate electronic transmission and possibly speed up response and recovery towards NH_3. Many reports claim that the doping of Py can also obtain the unique morphology of PPy with a large specific surface area, thus obtaining a large number of gas active sites.[33–36] In addition, PPy exhibits greater gas adsorption capacity and improves gas sensing applications by tweaking the morphology and structure of nanofibers, nanorods, nanowires, nanosheets or nanotubes to increase its specific surface area.[37,38] More notably, in addition to providing a large specific surface area for large gas active sites, one-dimensional (1-D) PPy nanostructure also provide a smooth electron transport channel for rapid gas adsorption and desorption and increase the conductivity for high gas sensitivity.[39] At present, there are many methods to prepare 1-D PPy nanomaterials.[40] Although template doping, including hard and soft templates, is an effective method to prepare one-dimensional PPy nanomaterials among many syntheses methods,[41,42] the template removal conditions in the hard template method are relatively harsh, thus prolonging the experimental period or even destroying nanostructures. Soft template method is easy to remove template agents, but may increase the cost and cause environmental pollution.[43] Therefore, developing a dopant that can not only manipulate the polymerization morphology of Py, but also improve the gas sensing performance of PPy, which is a problem that needs to be broken.

Metal phthalocyanine (MPc), as an organic large ring P-type semiconductor material, is the most famous gas sensing materials with room temperature operation, fast response and unique selectivity due to their 18 π-electron conjugated structure, active center metal and a variety of peripheral functional substituents.[44–46] Fortunately, the peripheral sulfonates ($-SO_3^{2-}$) and carboxylate ($-COO^-$) substituted MPcs can be easily prepared, which provides the possibility for phthalocyanine to be used as dopant to regulate morphology and improve the gas sensitivity of PPy.[47,48] It has been reported that PPy hydrogel are prepared by a water-soluble sodium sulfonate copper phthalocyanine as a template using the electrostatic interaction between the sulfonic acid group and Py, this uniform 1-D PPy hydrogel enhances the specific surface area and the electrical conductivity of PPy.[49,50] On the one hand, the proton base groups in phthalocyanine and the space structure of MPcs macrocycle induce the directed polymerization of Py monomers into nanostructures, and the PPy nanomaterials with unique morphology are obtained, resulting in higher gas adsorption capacity than the bulk PPy. On the other hand, substituted MPcs as anion doping improves the order of PPy microstructure, thus improving the conductivity of PPy. In addition, the active sites of O^{2-} generated by the central metal in MPcs facilitates the NH_3 selective adsorption.[51,52] Obviously, the NH_3-sensing properties of PPy-MPcs hybrids will be improved.

Based on the above exploration and research, in this paper, a water-soluble tetra-β-carboxylate cobalt phthalocyanine tetrasodium salt (TcCoPcTs) doped polypyrrole (PPy-TcCoPc) hybrid was prepared. The carboxylate ($-COO^-$) groups of TcCoPc are used as an organic anion dopant template, which links TcCoPc and positive radical of oxidized Py to form PPy-TcCoPc monomer salts by the electrostatic interaction. These PPy-TcCoPc monomer salts continue to polymerize over and over to form PPy nanorods. The effects of reaction ratio of TcCoPcTs, the reaction time and temperature on PPy-TcCoPc morphology were explored. In particular, the correlation between concentration of TcCoPc and conductivity and NH_3 sensing performance has been studied systematically. Ultimately, the resulted PPy-0.5TcCoPc sensor with a 3-D network, higher specific surface area and electrical conductivity shows a high gas response up to 49.3% for 50 ppm NH_3, accompanied by 8.1 s ultra-fast response speed, fast recovery ability and very low LOD of 8.1 ppb. Corresponding important parameters (including selectivity, reproducibility and humidity resistance) of the gas sensors and the response mechanism between PPy-TcCoPc and NH_3 gas were also tested and analysed.

Experimental

Reagents

Pyrrole (Py, 99% purity), isopropyl alcohol (purity, ≥99%), ammonium persulfate (APS, purity, >98%) were purchased from Sigma-Aldrich LLC. The ultra-pure water is produced by Millipore Milli-Q Water System (Bedford, MA, USA). Detailed synthesis steps of tetra-β-carboxylate cobalt phthalocyanine tetrasodium salt (TcCoPcTs) were listed in the support materials (see the ESI).† All chemical reagents were of analytical grade, and were used without further processing.

Preparation of PPy-TcCoPc hybrids

The freshly distilled Py monomer (1.2 mmol) was dissolved in 2 mL of isopropanol and recorded as group A. Different amounts of TcCoPcTs (the molar ratio of Py to TcCoPcTs was 40 : 1.0, 40 : 0.5 and 40 : 0.25, respectively) and ammonium persulphate (APS, 1 : 1 molar ratio to Py) were dissolved in 4 mL ultra-pure water and recorded as group B. All the above solutions were under the condition of 0–5 °C ice bath. The group B were added to group A and continuously stirred for 8 hours under an ice bath. The final reaction solution was filtered and the filter cake was washed successively with anhydrous ethanol and ultra-pure water until colorless. The PPy-TcCoPc black powder was dried for 2 h at 60 °C. The PPy-TcCoPc hybrids synthesized with different molar ratios of Py to TcCoPcTs (40 : 1.0, 40 : 0.5 and 40 : 0.25) were distinguished as PPy-1.0TcCoPc, PPy-0.5TcCoPc and PPy-0.25TcCoPc, respectively.

As a control, PPy was prepared without the addition of TcCoPcTs (see ESI†). The PPy/0.5TcCoPc hybrid was prepared by the same preparation process as PPy-0.5TcCoPc hybrid, except that tetra-β-carboxylate cobalt phthalocyanine (TcCoPc) was used instead of TcCoPcTs (see ESI†).

Sensors assembling and sensing measurement

The interdigital electrodes (IDEs) were used as load substrates for sensing materials, and ethanol was used as the solvent to prepare 0.5 mg mL^{-1} PPy-TcCoPc dispersion and ultrasonically dispersed for 30 min. Then, a minute amount of the solution was drop-coated on the IDEs surface and dried for 2 h at 50 °C to form a uniform and stable sensor. As controls, the PPy, TcCoPc, and PPy/TcCoPc hybrid sensors were assembled by the same process as PPy-TcCoPc sensor.

The NH_3-sensing parameters of the sensors were statically measured under the conditions of room temperature (20 ± 0.5 °C) and relative humidity of 50 ± 2% RH in a homemade gas sensor device. The air and commercially purchased high-purity NH_3 were used as blend and test gases, respectively (Dalian Guangming Gas Co., Ltd, China). The IDEs sensor containing the sensing hybrid was places in a self-made test container (total volume was 3 L), the initial resistance baseline was recorded in the air for a period, then the certified concentration of NH_3 was injected and the test was started. The data of resistance change was recorded. The closed sensing test container was released after the response was stable for a period, NH_3 was volatilized, and the spontaneous inflow of fresh air caused the resistance of the sensor down to its initial value. The humidity effect of the sensor was measured by subjecting the closed chamber to humidity changes with different kinds of saturated salt solutions (11.3% RH of LiCl, 33.3% RH of $MgCl_2$, 54.3% RH of $Mg(NO_3)_2$, 75.5% RH of NaCl, 85.1% RH of KCl and 94.6% RH of KNO_3, respectively) at 20 ± 0.5 °C.[53,54] Besides, the response was calculated as: $(R_g - R_a)/R_a \times 100\% = \Delta R/R_a \times 100\%$. Where R_a and R_g are the resistance values of the sensing device in air and in NH_3, respectively.[55,56] The response and recovery time are defined as the time required for 90% of the change in the resistance value of the sensing device when the NH_3 gas was injected into and removed from the test chamber, respectively.[57]

Characterization

Scanning electron microscopy (SEM) images were scanned by a S-4800 SEM (Hitachi, Japan). Transmission electron microscopy (TEM) images were observed by a JEM-2010 TEM (JEOL, Japan). UV-vis spectra from UV-2700 (Shimadzu, Japan), Fourier transform infrared spectra (FT-IR) from spectrum one spectrometer (PerkinElmer, USA), and Raman spectra with excitation wavelength of 633 nm from HR800Raman spectrophotometer (Jobin Yvon, France) were used for structural characterization. Specific surface areas were obtained using a Tristar 3020 (Micromeritics, USA) at 77 K and calculated by Brunauer–Emmett–Teller (BET) method. X-ray photoelectron spectroscopy (XPS) spectra were obtained using an AXIS Ultra DLD spectrometer (1235.6 eV, the monochromatic of Mg Kα source). The content of TcCoPc was quantitatively analysed by atomic absorption spectrometer (AAS, PinAAcle 900, PerkinElmer). Current–voltage curves (*I–V*) of IDEs sensing devices were determined by the two-point probe method (scan rate: 0.01 V s^{-1}, scan range: −1 to +1 V) (Keithley 4200).

Results and discussion

Preparation and characterization of the PPy-TcCoPc hybrids

The morphologies of PPy-TcCoPc hybrid were investigated by SEM and TEM. It can be seen from Fig. 1 that the PPy-0.5TcCoPc hybrid network structure was formed, which is composed of nanorods with a diameter of about 130 nm interlacing with each other. In contrast, under the same conditions, the PPy without TcCoPcTs doping only shows a disorderly agglomerated structure (Fig. S1†). Further observation revealed that the surface of the PPy-0.5TcCoPc nanorod contains some irregular tiny particles, which may be formed by PPy aggregation during rod formation. The TEM images result also show the same phenomenon (Fig. 1C and D). Unsurprisingly, the microstructure of PPy NPs has been optimized and changed to PPy nanorods because of the anion doping of TcCoPcTs to PPy.[36,58] This interlacing nanorod network structure is beneficial for providing a larger specific surface area, porosity and active site, and favours an enhanced gas adsorption activity. This improvement of microstructure was also demonstrated by the N_2 adsorption–desorption analysis (Fig. S2 and Table S1†). The results show the specific surface area of PPy-TcCoPc hybrids is increased, especially in PPy-0.5TcCoPc nanorods, its specific surface area (66.94 m^2 g^{-1}) increases 1.5-fold compared with PPy NPs (43.62 m^2 g^{-1}). As expected, the pore volume and average diameter size of PPy-0.5TcCoPc have also been improved (Table S1†). The PPy-TcCoPc hybrid nanorod network structure was obtained by manipulating of TcCoPcTs may facilitate the improvement of adsorption sites towards NH_3 gas.[59,60]

To further demonstrate the regulatory role of TcCoPcTs in preparing nanorods, the effects of TcCoPcTs dosage on preparing PPy nanorods were investigated. Fig. S3† indicates that the content change of TcCoPcTs plays an important

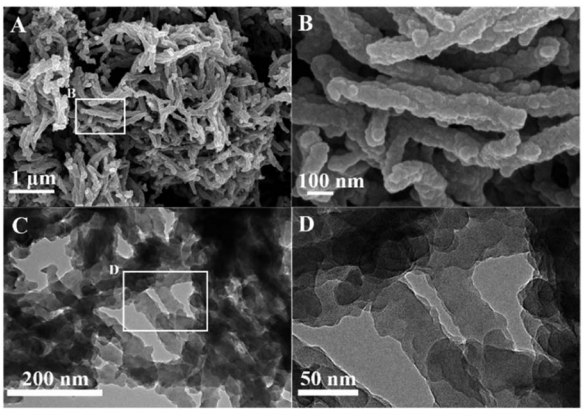

Fig. 1 SEM (A, B) and TEM (C, D) of PPy-0.5TcCoPc hybrid.

influence on the morphology of PPy-TcCoPc. As the mass ratio of Py and TcCoPcTs decreased (from 40 : 1.0 to 40 : 0.25), the diameter of PPy-TcCoPc rod increased. It can be understood that the diameter of PPy-TcCoPc nanorods decreases with the increase in TcCoPc content, which is similar to previous studies.[49,61] It is also further indicated that TcCoPcTs as a dopant, is an effective anionic doped molecule for ordered polymerization of Py due to the electrostatic interaction between the two. The morphology of PPy-TcCoPc hybrid was also affected by the synthesis temperature. As shown in Fig. S4,† the aggregation phenomenon of PPy-0.5TcCoPc hybrid polymerized at room temperature is more serious, and its length is also shorter than that at low temperature (0–5 °C). In addition, the TcCoPc content of three kinds of PPy-0.25TcCoPc, PPy-0.5TcCoPc and PPy-1.0TcCoPc hybrids was quantitatively analysed using the standard curve method with cobalt standard solution by atomic absorption spectroscopy (AAS, Fig. S5 and Table S2†). The analysis revealed that the content of TcCoPc in PPy-0.25TcCoPc, PPy-0.5TcCoPc and PPy-1.0TcCoPc hybrids is 7.25%, 17.2% and 20.8%, respectively.

The change of morphology of PPy-0.5TcCoPc nanorods with reaction time was observed to verify its formation mechanism (Fig. S6†). Obviously, when the polymerization time is less than 2 minutes, the hybrid still exhibits the morphology of disordered microspheres (Fig. S6A†). With the observation of the reaction process, the reaction solution also changed from dark blue (the colour of TcCoPc) to black (the colour of PPy), and also from fluid to hydrogel. When the polymerization time continued to 10 minutes, the PPy-TcCoPc nanorods were formed (Fig. S6B†). Then, as the polymerization time increases, the PPy-TcCoPc nanorods become longer and dispersed, intertwine and form a network structure, but the change is no longer significant after 8 h of reaction. Observing the above results, the possible formation mechanism of PPy-TcCoPc nanorods can be demonstrated by Scheme 1. First, the alkaline –COO^- group of TcCoPcTs and the acidic $^{+\cdot}$N–H of Py can be linked to form Py-TcCoPcTs monomer salts by electrostatic interaction. With the addition of APS, these salts rapidly undergo directional polymerization as reaction units. Ultimately, TcCoPcTs, as a tetrameric dopant, polymerized along the pyrrole chain with its supramolecular self-loading interaction to form 1-D PPy-TcCoPc nanorods.

To further demonstrate the role and successful doping of TcCoPcTs in the preparation of PPy-TcCoPc hybrid, the PPy-TcCoPc hybrid was analysed by UV-vis, FT-IR and Raman spectra (Fig. 2A–C, S7 and S8).† The corresponding UV-vis spectra of PPy NPs, TcCoPc and PPy-TcCoPc hybrids dissolved in DMF are shown in Fig. 2A and S7A, B.† In addition to preserving the basic characteristics absorption of PPy (415 nm), the characteristics Q-band absorption of TcCoPc (686 nm) is obviously found in PPy-TcCoPc hybrid, and the intensity of absorption peak increases with the increase of TcCoPc content (Fig. S7A and B†). Moreover, this new peak is red-shifted by 18 nm due to the electrostatic interaction between PPy and

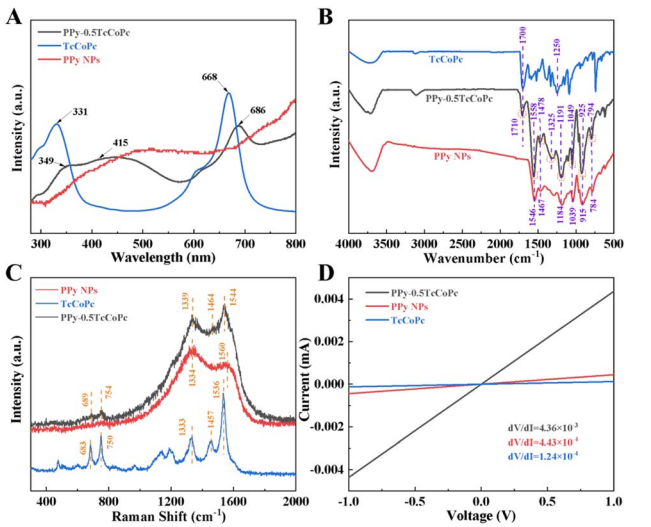

Fig. 2 (A) UV-vis spectra, (B) FT-IR spectra, (C) Raman spectra (λ_{exc} = 633 nm) and (D) *I*–*V* curves of PPy NPs, TcCoPc and PPy-0.5TcCoPc hybrid, respectively.

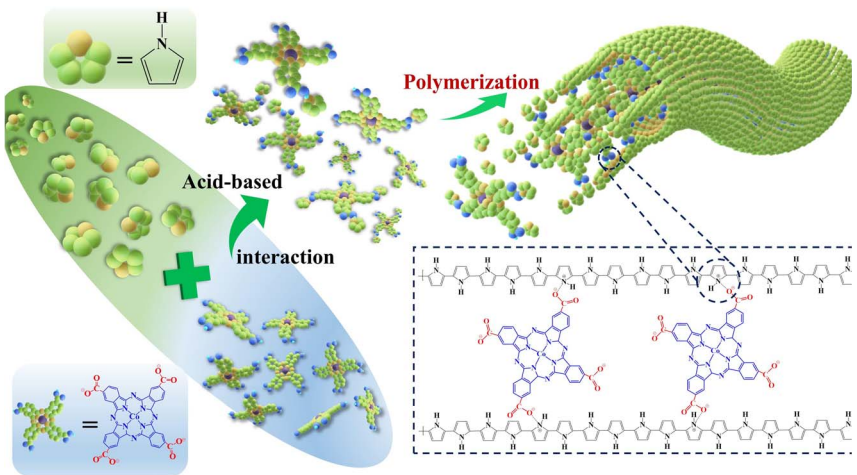

Scheme 1 Concise schematic of the procedure of PPy-TcCoPc hybrid formation process.

TcCoPcTs.[62] Similar results can be obtained in the FT-IR spectra (Fig. 2B and S7C†). Compared with PPy NPs, the new peaks at 1325 cm^{-1} and 1710 cm^{-1} (C–O and C═O of –COOH) derived from TcCoPc are found from PPy-0.5TcCoPc hybrid in the FT-IR spectra. Moreover, the typical peaks of PPy at 1558 and 1478 cm^{-1} (the C═C bond and the C–N bond) also appear in the PPy-0.5TcCoPc hybrid.[63,64] Meanwhile, the doping and polymerized states of PPy are represented by 1191, 1049, 925 and 794 cm^{-1} with a certain shift, respectively.[65,66] The doping of TcCoPc can be further evidenced from the Raman spectra (Fig. 2C and S8†). The two main peaks of PPy at 1560 and 1334 cm^{-1} derived from the PPy ring and the C═C backbone vibrations, respectively.[67,68] When TcCoPc is doped into PPy, the typical characteristic peaks at 1536 cm^{-1} (aromatic C–N bond), 1457 cm^{-1} (C═C pyrrole stretching) and 1333 cm^{-1} (aromatic C–C bond) derived from TcCoPc are shifted to 1544, 1464 and 1339 cm^{-1} in PPy-0.5TcCoPc hybrid.[69,70] Besides, two new peaks at 754 and 689 cm^{-1} (assigned to aromatic atoms vibrating in out-of-macrocyclic-ring vibrational modes) are also observed in PPy-TcCoPc hybrid.[71] These new peaks and their shift indicate that Py and TcCoPcTs can be linked by the electrostatic interaction. The FT-IR and Raman spectra of PPy-0.25TcCoPc and PPy-1.0TcCoPc hybrids are similar to that of PPy-0.5TcCoPc hybrid, except the peak intensity changes significantly with the increase of TcCoPc content (Fig. S7 and S8†).

The morphology change and anionic doping of the conductive polymer will affect the conductivity of the polymer.[72] Fig. 2D and S9† show the *I–V* curve of PPy NPs, TcCoPc and PPy-TcCoPc hybrids. Compared to the pristine PPy NPs and TcCoPc, the conductivity of PPy-TcCoPc hybrid is enhanced, especially in PPy-0.5TcCoPc hybrid, because of enhanced interchain charge transport of TcCoPc doped PPy. All results indicate that the PPy-0.5TcCoPc hybrid prepared by this suitable molar ratio of Py and TcCoPcTs obtains the superior morphology, large specific surface area, good electrical conductivity and charge transport channel, which may improve the gas-sensing performance of PPy-0.5TcCoPc hybrid towards NH_3.

To further analyse the relationship between the PPy and TcCoPc, XPS measurements were performed. Fig. 3 shows the survey XPS spectra of PPy NPs, TcCoPc and PPy-0.5TcCoPc. In addition to the N 1s, O 1s and C 1s peaks, the Co 2p peak is also clearly found in the survey spectrum of PPy-0.5TcCoPc hybrid, which confirms TcCoPc was successfully doped into PPy. The C 1s XPS spectrum for the PPy NPs can be decomposed into four component peaks, which represent β carbon atoms (283.68 eV), α carbon atoms in the Py ring (284.8 eV), the $=C–N^{\cdot+}$ bond of PPy polarons (286.19 eV) and the $–C=N^{+}$ of bipolaron charge carrier species (287.51 eV), respectively.[73] When TcCoPc is doped into PPy, the peak at 286.21 eV ($=C–N^{\cdot+}$) of PPy disappears, and the new peaks at 285.92 eV ($C–O^{-}$) appear in the PPy-0.5TcCoPc hybrid derived from TcCoPc. Meanwhile, the new peaks at 289.88 eV (C═O) also appear and shift by 1.08 eV compared with TcCoPc.[74] It indicates that the $–COO^{-}$ group of TcCoPcTs is doped to PPy by the electrostatic interaction (the inset image (a) in Fig. 3). Similarly, the ═NH– bond at 397.59 eV and the –NH– bond at 399.46 eV are red-shifted by 0.16 eV and 0.06 eV relative to the PPy in the N 1s XPS spectrum of PPy-0.5TcCoPc hybrid, respectively.[75,76] All results further evidence that TcCoPcTs is successfully linked into PPy to form the PPy-0.5TcCoPc hybrid based on electrostatic interactions.

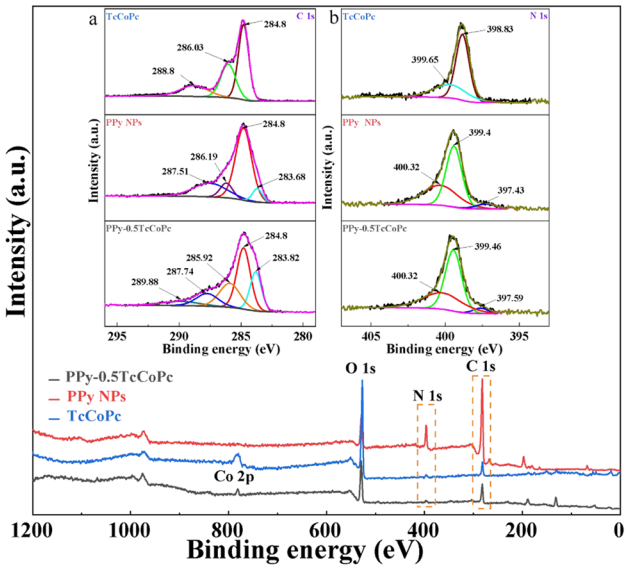

Fig. 3 XPS spectra of PPy NPs, TcCoPc and PPy-0.5TcCoPc (inside: (a) C 1s and (b) N 1s XPS of PPy NPs, TcCoPc and PPy-0.5TcCoPc).

NH_3-sensing properties of PPy-TcCoPc hybrids

According to the previous design, adding TcCoPcTs into PPy as an anionic dopant will play a chemical synergy between the two, not only optimizing the morphology and improving the conductivity, but also improving the NH_3-sensing of the PPy-TcCoPc hybrids. This can be well supported by comparing the sensing properties of PPy-TcCoPc hybrids and control groups

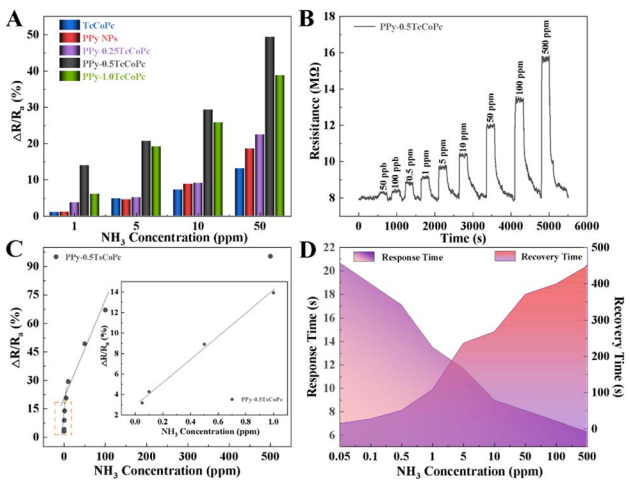

Fig. 4 (A) NH_3-sensing response of PPy NPs, TcCoPc and PPy-0.5TcCoPc sensors. (B) Response and recovery curves of PPy-0.5TcCoPc sensor under different NH_3 concentration. (C) Response time and recovery time of PPy-0.5TcCoPc upon exposure to 0.05–500 ppm NH_3. (D) Relationship between NH_3 concentration change and PPy-0.5TcCoPc sensor response at room temperature (20 °C).

(PPy NPs, TcCoPc) to NH_3 (Fig. 4A, S10 and Table S3†). Fig. 4A shows that although the TcCoPc sensor has a certain response for NH_3, it is difficult to measure because of the problem of high resistance. In addition, PPy NPs sensor also shows a lower response similar to TcCoPc, shows a better response/recovery performance (Fig. S10†). In contrast, the PPy-TcCoPc sensors show a greater breakthrough in NH_3-sensing performance compared with the PPy NPs and TcCoPc, especially the PPy-0.5TcCoPc sensor has the highest NH_3-sensing response, the fastest response and recovery time (49.32%, 8.1 s and 370.8 s under 50 ppm). Besides, the response of the PPy-0.5TcCoPc sensor under different polymerization times to 100 ppm NH_3 was also explored. It is observed that the PPy-0.5TcCoPc sensor with a polymerization time of 8 h presents the highest response to NH_3 (Fig. S11†). Therefore, the NH_3-sensing properties of PPy-0.5TcCoPc sensor has been systematically studied in detail in Fig. 4B–D. Fig. 4B shows the response and recovery curve of the PPy-0.5TcCoPc sensor under 9 cycles NH_3 concentration at room temperature. The PPy-0.5TcCoPc sensor still exhibits fast response and good recovery speed at 50 ppb NH_3 concentration, accompanied by excellent response (3.18% to response value, 20.7/14.4 s to response/recovery time).

Moreover, Fig. 4C also shows that the response speed of the PPy-0.5TcCoPc sensor was also accelerated than that of PPy NPs and TcCoPc, and faster response times were also obtained as NH_3 concentration increased. At the same time, there are two good linear relationships between its response and NH_3 concentration in Fig. 4D: high slope rises in the 0.05–1 ppm concentration area (11.1% per ppm), and a slow rise in the high concentration region of 5–100 ppm (0.47% per ppm).[77] The lowest theoretical limit of detection (LOD) of PPy-0.5TcCoPc for NH_3 was calculated by formula (1) and (2) is about 8.1 ppb (S/N = 3) (Table 1) (ESI showed the formula meaning and calculation process in detail†).[78–80] The excellent response, limit of detection and fast response time coupled with good recovery time of the PPy-0.5TcCoPc hybrid make it stand out among many room temperature gas sensing materials (Table S4†). Therefore, the incorporation of TcCoPcTs into PPy by electrostatic interaction can not only trigger the orderly polymerization of PPy, optimize the morphology and increase the specific surface area, but also NH_3-sensing performance can be greatly enhanced, broaden the scope of application.

$$\mathrm{LOD_{ppm}} = 3 \times \frac{\mathrm{RMS_{noise}}}{\mathrm{slope}} \quad (1)$$

$$\mathrm{RMS_{noise}} = \sqrt{\frac{S^2}{N}} \quad (2)$$

Other important performance parameters of the PPy-0.5TcCoPc sensor were also tested, including reproducibility, stability, humidity tolerance and gas selectivity (Fig. 5). Fig. 5A shows that the comparative analytical of the PPy-0.5TcCoPc, PPy NPs and TcCoPc sensors for selectivity to other 50 ppm inorganic gases (including NH_3) and 10 000 ppm volatile organic compounds. PPy sensor has a certain response to NH_3 due to the unique redox reaction between PPy and NH_3, but PPy also has the ability to exchange protons for other inorganic gases,[81] which makes it poor selectivity. Compared with PPy, the presence of active center metals in TcCoPc enables itself to show better selectivity for NH_3. But because there are fewer active sites, it has a lower response. These deficiencies can be overcome by TcCoPc doped into PPy, and excellent selectivity towards NH_3 is clearly observed in the PPy-0.5TcCoPc sensor. Fig. 5B depicts the response of the PPy-0.5TcCoPc sensor to 7 consecutive cycles of 10 ppm NH_3 has no obvious change, showing good reproducibility. In addition, when the PPy-0.5TcCoPc sensor was placed in an air environment for 45 days, its response to 10 ppm and 50 ppm NH_3 was tested every 5 days, resulting in a decrease of only 3.6% and 2.8%, respectively (Fig. 5C). In order to further verify the shelf life of the PPy-0.5TcCoPc sensor, the PPy-0.5TcCoPc sensor placed for 3, 6 and 9 months was tested. The comparison diagram of its

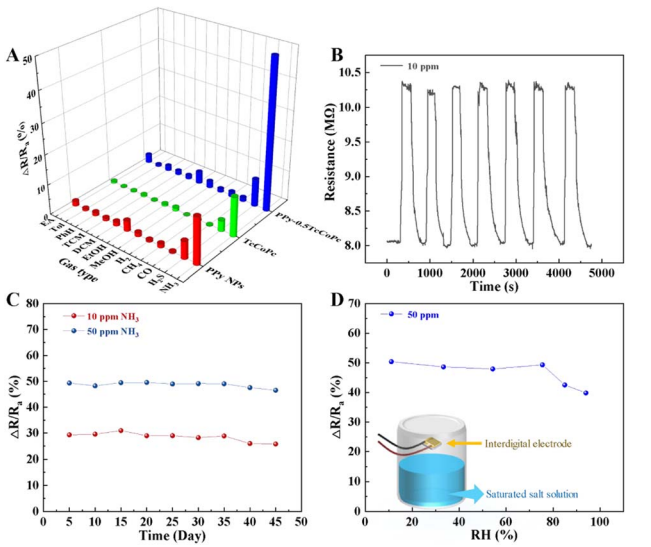

Fig. 5 (A) Comparative analysis of selectivity of PPy NPs, TcCoPc and PPy-0.5TcCoPc sensors; (inside: EA, Tol, PhH, TCM, DCM, EtOH and MeOH represent ethyl acetate, toluene, benzene, trichloromethane, dichloromethane, ethanol and methanol, respectively). (B) Reproducibility of the PPy-0.5TcCoPc sensor for 7 cycles of 10 ppm NH_3. (C) Long-term stability of the PPy-0.5TcCoPc sensor at 10 ppm and 50 ppm of NH_3. (D) Response of the PPy-0.5TcCoPc sensor to 50 ppm of NH_3 under different relative humidity (RH) conditions at room temperature (20 °C).

Table 1 Relationship between the change of NH_3 concentration and the response of PPy-0.5TcCoPc sensor

Sensing material	The concentrations ranging of NH_3 is from 0.05 to 1 ppm	The concentrations ranging of NH_3 is from 10 to 100 ppm	Limit of detection (LOD)
PPy-0.5TcCoPc	$Y = 11.1x + 2.99$ ($R^2 = 0.993$)	$Y = 0.47x + 22.37$ ($R^2 = 0.956$)	8.1 ppb

response to NH_3 gas is shown in Fig. S12.† It can be seen from the figure that the sensor has a good shelf life in the range of 6 months in terms of sensitivity to NH_3 gas. The effect of humidity on the PPy-0.5TcCoPc sensor was also monitored. Fig. 5D shows that the PPy-0.5TcCoPc sensor is relatively stable in a wide humidity range from 11.1 to 75.0% RH. This can be applied in most environmental conditions.

The sensing mechanism of the PPy-0.5TcCoPc sensor

The charge transfer between PPy, TcCoPc and gas molecular, as semiconductor gas-sensing materials, is a recognized gas-sensing mechanism.[82,83] Therefore, improving their electrical conductivity, active site and interaction force with gas molecules are effective pathway to induce NH_3-sensing.[84] The rapid response/recovery capabilities and high sensitivity of the PPy-TcCoPc hybrids are derived from the synergistic effects of TcPcCo, and PPy (as described in Scheme 2). In the air, due to the presence of TcPcCo in the PPy, the free-flowing oxygen molecules can rapidly and spontaneously adsorb on the center metal atoms of TcPcCo, which further capture electrons, forming adsorbed oxygen species (O_2^-). When the PPy-TcCoPc hybrids are exposed to NH_3 flow, similar to the case of all hybrids of PPy, a redox reaction occurs between PPy and NH_3 (as described in eqn (3) and (4)), and electrons are transferred from the NH_3 molecule to the PPy main chains.[85] In addition, the NH_3 molecules react with the pre-chemisorbed O_2^-, thus releasing a large number of electrons as indicated in the following equation: $4NH_3(g) + 3O_2^-(ads) \rightarrow 2N_2(g) + 6H_2O(g) + 6e^-$.[86] The abovementioned two processes occur simultaneously and lead to the reduction of charge carriers of the PPy-TcCoPc hybrids.[87,88] Contrary to the response process, the PPy-TcCoPc hybrids can lose electrons quickly by reacting with the reappearing oxygen molecules, and the resistance of the PPy-TcCoPc hybrid gradually returns to the initial baseline.

$$PPy^+ + NH_3 \rightarrow PPy^0 + NH_4^+ \text{ adsorption} \quad (3)$$

$$PPy^0 + NH_4^+ \rightarrow PPy^+ + NH_3 \text{ desorption} \quad (4)$$

The above sensing performance of PPy-0.5TcCoPc hybrid can be verified by XPS O 1s and N 1s spectra. Fig. 6A shows that the O_2^- content in the PPy-0.5TcCoPc hybrid rapidly decreases by up to 13.7%, which means that O_2^- reacts with NH_3 when exposed to NH_3 atmosphere. Moreover, from the high-resolution N 1s XPS spectra in Fig. 6B, the content of $-NH^{\cdot+}-$ decreases obviously while the content of –NH– increases when the PPy-0.5TcCoPc hybrid is exposed to NH_3. This further proves the redox process between PPy and NH_3, which is reflected in the protonation change of –NH–. In addition, the nanorod structure of the PPy-0.5TcCoPc hybrid formed by the regulation of TcCoPcTs greatly increases its specific surface area, thus increasing the active site of interaction between the PPy-0.5TcCoPc sensor and NH_3, and improving the response to NH_3. Therefore, once the composite is exposed to NH_3, the generated electrons can be transmitted effectively, resulting in rapid response and recovery speed.

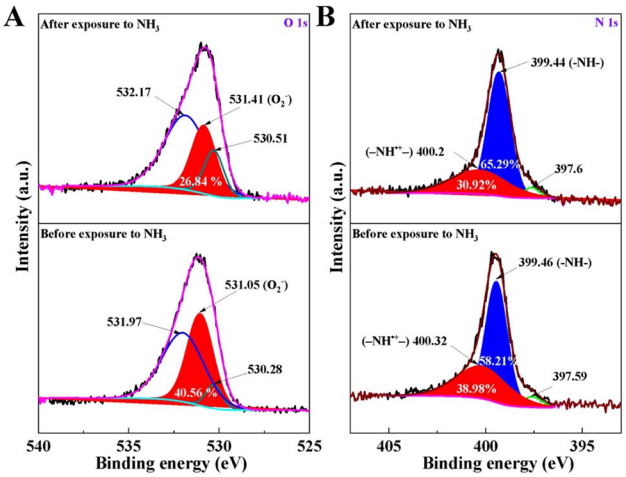

Fig. 6 Effects of NH_3 exposure on changes in XPS spectra of the PPy-0.5TcCoPc sensor high-resolution (A) O 1s and (B) N 1s.

To further demonstrate the role of TcCoPcTs in the NH_3-sensing performance of the doped PPy-TcCoPc. Through the similar preparation method of PPy-0.5TcCoPc, only TcCoPc is used to replace TcCoPcTs, PPy/0.5TcCoPc hybrid was prepared and characterized by UV-vis, FT-IR and SEM (see ESI† for the synthesis process). SEM results show that PPy/0.5TcCoPc hybrid only shows a disorderly agglomerated structure similar to PPy NPs, but does not form nanorod structure (Fig. S13†). The NH_3-sensing results show that although PPy/0.5TcCoPc hybrid shows good response and recovery speed similar to PPy-0.5TcCoPc, its response to NH_3 is significantly lower than PPy-0.5TcCoPc (Fig. S14A–C†). It can be seen from the *I–V* curve in the Fig. S15A,† the conductivity of PPy/0.5TcCoPc hybrid is 2.7 times smaller than that of PPy-0.5TcCoPc hybrid. The BET results also show that the specific surface area of PPy/0.5TcCoPc (59.96 $m^2\ g^{-1}$) was 1.12 times smaller than that of PPy-0.5TcCoPc (66.94 $m^2\ g^{-1}$), lower numerical of pore volume and average diameter size (Fig. S15B and Table S5).† Therefore, the NH_3-sensing performance of PPy-0.5TcCoPc is significantly better than that of PPy/0.5TcCoPc hybrid. This further confirms that the improvement of the morphology and conductivity of the hybrid mainly comes from the anionic doping of TcCoPcTs,[89] which plays a vital role in enhancing the NH_3-

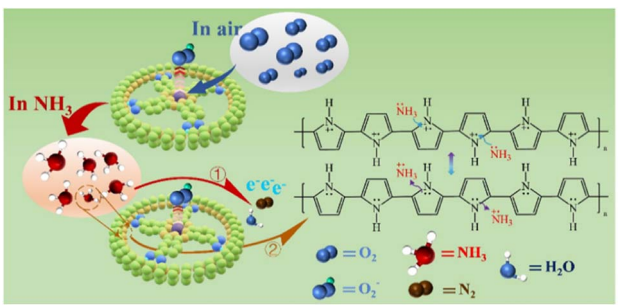

Scheme 2 Response mechanism of the PPy-TcCoPc sensor to NH_3.

sensing performance. Based on the above, TcCoPcTs can not only be used as an anionic dopant to adjust the micromorphology, increase the specific surface area of PPy and increase the active site to NH_3, and improve its conductivity and accelerate charge transfer, combined with the response of PPy to NH_3. PPy-0.5TcCoPc hybrid exhibits fast response/recovery speed, high response and specific selectivity for NH_3.

Conclusions

In conclusion, PPy-0.5TcCoPc nanorod was successfully prepared by phthalocyanine anion doping. The prepared PPy-0.5TcCoPc hybrid showed fast response speed, high response value, better stability and selectivity of NH_3-sensing properties. The unique 3-D network nanorod structure with high specific surface area and electrical conductivity, the synergistic optimization of PPy and TcCoPc provides more active sites for NH_3, stronger interaction with NH_3, faster electron diffusion and transmission speed. This work provides a new approach to control the morphology, conductivity and gas-sensing of polymers using phthalocyanine doping, and further expands the application of phthalocyanines and conducting polymers in gas sensors.

Author contributions

Shijie Gai: investigation, methodology, writing – original draft. Bin Wang: conceptualization, project administration. Xiaolin Wang: resources. Runze Zhang and Kun Zeng: investigation, validation. Shoulei Miao: writing – review & editing. Yiqun Wu: supervision.

Conflicts of interest

There are no conflicts to declare.

Acknowledgements

We gratefully acknowledge financial support from the National Natural Science Foundation of China (51202061), Heilongjiang Provincial Natural Science Foundation of China (LH2019E076), and the Innovative Talents Program of Harbin (2017RAQXJ143).

Notes and references

1 N. M. Nurazzi, S. Z. N. Demon, N. A. Halim, I. S. Mohamad and N. Abdullah, *Polimery*, 2021, **66**, 175–186.
2 S. Sardana, H. Kaur, B. Arora, D. K. Aswal and A. Mahajan, *ACS Sens.*, 2022, **7**, 312–321.
3 A. H. Ismail, N. A. M. Yahya, M. H. Yaacob, M. A. Mahdi and Y. Sulaiman, *Synth. Met.*, 2020, **260**, 116294.
4 J. M. He, B. Y. Liang, X. J. Yan, F. M. Liu, J. Wang, Z. J. Yang, R. You, C. G. Wang, P. Sun, X. Yan, H. Z. Lin, B. N. Kang, Y. Wang and G. Y. Lu, *Sens. Actuators, B*, 2021, **327**, 128940.
5 Y. Yin, H. T. Zhang, P. R. Huang, C. L. Xiang, Y. J. Zou, F. Xu and L. X. Sun, *Mater. Res. Bull.*, 2018, **99**, 152–160.
6 M. D. Fernandez-Ramos, L. F. Capitan-Vallvey, L. M. Pastrana-Martinez, S. Morales-Torres and F. J. Maldonado-Hodar, *Sens. Actuators, B*, 2022, **368**, 132103.
7 M. S. Pawar and D. J. Late, *Beilstein J. Nanotechnol.*, 2019, **10**, 467–474.
8 A. S. Pawbake, S. R. Jadkar and D. J. Late, *Mater. Res. Express*, 2016, **3**, 105038.
9 M. Pawar, S. Kadam and D. J. Late, *ChemistrySelect*, 2017, **2**, 4068–4075.
10 M. B. Erande, M. S. Pawar and D. J. Late, *ACS Appl. Mater. Interfaces*, 2016, **8**, 11548–11556.
11 D. J. Late, T. Doneux and M. Bougouma, *Appl. Phys. Lett.*, 2014, **105**, 233103.
12 D. J. Late, Y. K. Huang, B. Liu, J. Acharya, S. N. Shirodkar, J. J. Luo, A. M. Yan, D. Charles, U. V. Waghmare, V. P. Dravid and C. N. R. Rao, *ACS Nano*, 2013, **7**, 4879–4891.
13 E. Gorbova, F. Tzorbatzoglou, C. Molochas, D. Chloros, A. Demin and P. Tsiakaras, *Catalysts*, 2022, **12**, 1.
14 A. Aaryashree, S. Sahoo, P. Walke, S. K. Nayak, C. S. Rout and D. J. Late, *Nano Res.*, 2021, **14**, 3669–3689.
15 H. Y. Tang, L. N. Sacco, S. Vollebregt, H. Y. Ye, X. J. Fan and G. Q. Zhang, *J. Mater. Chem. A*, 2020, **8**, 24943–24976.
16 B. J. Mueller, N. Steinmann, S. M. Borisov and I. Klimant, *Sens. Actuators, B*, 2018, **255**, 1897–1901.
17 D. J. Late, R. V. Kanawade, P. K. Kannan and C. S. Rout, *Sens. Lett.*, 2016, **14**, 1249–1254.
18 M. S. Pawar, S. R. Kadam, B. B. Kale and D. J. Late, *Nanoscale Adv.*, 2021, **3**, 4799–4803.
19 S. Sharma, R. Saini, G. Gupta and D. J. Late, *Nanotechnology*, 2023, **34**, 045704.
20 V. S. Bhati, M. Kumar and R. Banerjee, *J. Mater. Chem. C*, 2021, **9**, 8776–8808.
21 D. J. Late and C. Wiemer, *AIP Adv.*, 2022, **12**, 110401.
22 H. Hoang Thi, T. Chu Van, T. Do Thi Anh, N. Pham Quang, T. Giang Hong, D. Sai Cong, G. Ho Truong, V. Nguyen Duc and T. Tran, *Synth. Met.*, 2019, **250**, 35–41.
23 S. J. Luo, J. L. Zhao, J. F. Zou, Z. L. He, C. W. Xu, F. W. Liu, Y. Huang, L. Dong, L. Wang and H. Zhang, *ACS Appl. Mater. Interfaces*, 2018, **10**, 3538–3548.
24 B. H. Liu, X. Y. Liu, Z. Yuan, Y. D. Jiang, Y. J. Su, J. Y. Ma and H. L. Tai, *Sens. Actuators, B*, 2019, **295**, 86–92.
25 J. Stejskal and J. Prokes, *Synth. Met.*, 2020, **264**, 116373.
26 R. S. Anwane, S. B. Kondawar and D. J. Late, *Mater. Lett.*, 2018, **221**, 70–73.
27 Y. X. Chen, W. Q. Zhang, C. K. She, G. S. Li, L. H. Zhang, S. H. Liu, Y. Cheng, C. B. Jing and J. H. Chu, *RSC Adv.*, 2019, **9**, 36351–36357.
28 M. Saghafi, M. Mahmoodian, S. A. Hosseini, A. Abdollahi and S. Mohajerzadeh, *Electrochim. Acta*, 2018, **283**, 1450–1459.
29 X. H. Zhang, S. S. Wang, S. Lu, J. Su and T. He, *J. Power Sources*, 2014, **246**, 491–498.
30 H. M. Hung, D. K. Linh, N. T. Chinh, L. M. Duc and Q. Trung, *Prog. Org. Coat.*, 2019, **131**, 407–416.
31 A. Fakhry, F. Pillier and C. Debiemme-Chouvy, *J. Mater. Chem. A*, 2014, **2**, 9859–9865.

32 M. Y. Zhang, Y. Song, D. Guo, D. Yang, X. Q. Sun and X. X. Liu, *J. Mater. Chem. A*, 2019, **7**, 9815–9821.
33 J. Stejskal and M. Trchova, *Colloid Polym. Sci.*, 2020, **298**, 319–325.
34 S. Sankar, K. Parvathi and M. T. Ramesan, *High Perform. Polym.*, 2020, **32**, 719–728.
35 J. Oh, J. S. Lee and J. Jang, *Polymers*, 2020, **12**, 1427.
36 K. H. Cho, J. Jang and J. S. Lee, *ACS Omega*, 2020, **5**, 2992–2999.
37 Y. C. Wong, B. C. Ang, A. Haseeb, A. A. Baharuddin and Y. H. Wong, *J. Electrochem. Soc.*, 2019, **167**, 037503.
38 H. Luo, Y. V. Kaneti, Y. Ai, Y. Wu, F. C. Wei, J. W. Fu, J. G. Cheng, C. B. Jing, B. Yuliarto, M. Eguchi, J. Na, Y. Yamauchi and S. H. Liu, *Adv. Mater.*, 2021, **33**, 2007318.
39 C. Bellaner Diaz-Arriaga, J. Martin Baas-Lopez, D. Esperanza Pacheco-Catalan and J. Uribe-Calderon, *Synth. Met.*, 2020, **269**, 116541.
40 J. P. Jyothibasu, M. Z. Chen and R. H. Lee, *ACS Omega*, 2020, **5**, 6441–6451.
41 L. J. Pan, H. Qiu, C. M. Dou, Y. Li, L. Pu, J. B. Xu and Y. Shi, *Int. J. Mol. Sci.*, 2010, **11**, 2636–2657.
42 I. M. Minisy, P. Bober, U. Acharya, M. Trchova, M. Hromadkova, J. Pfleger and J. Stejskal, *Polymer*, 2019, **174**, 11–17.
43 J. P. Jyothibasu and R. H. Lee, *J. Mater. Chem. A*, 2020, **8**, 3186–3202.
44 B. Wang, X. L. Wang, Z. J. Guo, S. J. Gai, Y. Li and Y. Q. Wu, *RSC Adv.*, 2021, **11**, 5993–6001.
45 X. D. Lu, Z. M. Chen, H. Wu, E. P. Cao, Y. Wang, S. C. Du, Y. Q. Wu and Z. Y. Ren, *J. Mater. Chem. A*, 2021, **9**, 4150–4158.
46 X. H. Liu, W. Zheng, R. Kumar, M. Kumar and J. Zhang, *Coord. Chem. Rev.*, 2022, **462**, 214517.
47 Z. L. Tang, J. Xiao, F. Li, Z. H. Ma, L. Wang, F. F. Niu and X. L. Sun, *ACS Omega*, 2020, **5**, 10451–10458.
48 A. Gunsel, A. T. Bilgicli, B. Barut, P. Taslimi, A. Ozel, Z. Biyiklioglu, M. N. Yarasir and I. Gulcin, *J. Mol. Struct.*, 2020, **1214**, 128210.
49 Y. Q. Wang, Y. Shi, L. J. Pan, Y. Ding, Y. Zhao, Y. Li, Y. Shi and G. H. Yu, *Nano Lett.*, 2015, **15**, 7736–7741.
50 Y. T. Meng, J. J. Yin, T. F. Jiao, J. H. Bai, L. X. Zhang, J. J. Su, S. F. Liu, Z. H. Bai, M. W. Cao and Q. M. Peng, *J. Mol. Liq.*, 2020, **298**, 112010.
51 H. Wu, Z. M. Chen, J. L. Zhang, F. Wu, C. Y. He, Y. Q. Wu and Z. Y. Ren, *J. Mater. Chem. A*, 2017, **5**, 24493–24501.
52 D. Gounden, N. Nombona and W. E. van Zyl, *Coord. Chem. Rev.*, 2020, **420**, 213359.
53 D. J. Late, *Microporous Mesoporous Mater.*, 2016, **225**, 494–503.
54 P. V. Shinde, S. Gagare, C. S. Rout and D. J. Late, *RSC Adv.*, 2020, **10**, 29378–29384.
55 L. D. Bharatula, M. B. Erande, I. S. Mulla, C. S. Rout and D. J. Late, *RSC Adv.*, 2016, **6**, 105421–105427.
56 K. Rajkumar and R. T. R. Kumar, in *Fundamentals and Sensing Applications of 2D Materials*, ed. M. Hywel, C. S. Rout and D. J. Late, Woodhead Publishing, 2019, pp. 205–258, DOI: 10.1016/B978-0-08-102577-2.00006-3.
57 A. Bag and N. E. Lee, *J. Mater. Chem. C*, 2019, **7**, 13367–13383.
58 J. Arroyo, M. Akieh-Pirkanniemi, G. Lisak, R. M. Latonen and J. Bobacka, *J. Membr. Sci.*, 2019, **581**, 50–57.
59 S. Q. Li, A. Liu, Z. J. Yang, J. M. He, J. Wang, F. M. Liu, H. Y. Lu, X. Yan, P. Sun, X. S. Liang, Y. Gao and G. Y. Lu, *Sens. Actuators, B*, 2019, **299**, 126970.
60 A. Aaryashree, P. V. Shinde, A. Kumar, D. J. Late and C. S. Rout, *J. Mater. Chem. C*, 2021, **9**, 3773–3794.
61 S. C. Hu, Y. Zhou, L. L. Zhang, S. J. Liu, K. Cui, Y. Y. Lu, K. N. Li and X. D. Li, *J. Mater. Sci.*, 2018, **53**, 3016–3026.
62 M. B. Lan, H. L. Zhao, H. H. Yuan, C. R. Jiang, S. H. Zuo and Y. Jiang, *Dyes Pigm.*, 2007, **74**, 357–362.
63 M. Chigondo, H. K. Paumo, M. Bhaumik, K. Pillay and A. Maity, *J. Mol. Liq.*, 2019, **275**, 778–791.
64 R. Y. Chen, J. Zhong, H. F. Zhu, C. M. Tang, Y. L. Qiao, C. Q. Fu, J. L. Wang, L. Shen, H. F. He and F. Gao, *Polym. Int.*, 2021, **70**, 1246–1254.
65 S. Peshoria and A. K. Narula, *J. Mater. Sci.*, 2018, **53**, 3876–3888.
66 C. P. Han, R. Y. Shi, D. Zhou, H. F. Li, L. Xu, T. F. Zhang, J. Q. Li, F. Y. Kang, G. X. Wang and B. H. Li, *ACS Appl. Mater. Interfaces*, 2019, **11**, 15646–15655.
67 G. Telipan, L. Pislaru-Danescu, E. M. Lungulescu, I. Ion and V. Marinescu, *Appl. Sci.*, 2021, **11**, 4168.
68 A. Arena, C. Branca, C. Ciofi, G. D'Angelo, V. Romano and G. Scandurra, *Nanomaterials*, 2021, **11**, 2589.
69 X. F. Zhang, W. H. Lin, H. F. Zhao and R. M. Wang, *Vib. Spectrosc.*, 2018, **96**, 26–31.
70 G. Giancane, E. Filippo, D. Manno, A. Serra and L. Valli, *J. Colloid Interface Sci.*, 2011, **363**, 199–205.
71 M. Wierzchowski, L. Sobotta, D. Lazewski, P. Kasprzycki, P. Fita and T. Goslinski, *J. Mol. Struct.*, 2020, **1203**, 127371.
72 J. H. Sun, X. Shu, Y. L. Tian, Z. F. Tong, S. L. Bai, R. X. Luo, D. Q. Li and A. F. Chen, *Sens. Actuators, B*, 2017, **238**, 510–517.
73 T. Yoon, J. Jun, D. Y. Kim, S. Pourasad, T. J. Shin, S. U. Yu, W. Na, J. Jang and K. S. Kim, *J. Mater. Chem. A*, 2018, **6**, 2257–2263.
74 H. Wu, Z. M. Chen, J. L. Zhang, F. Wu, C. Y. He, Z. Y. Ren and Y. Q. Wu, *Chem. Mater.*, 2017, **29**, 9509–9517.
75 F. C. Wei, Y. H. Zhong, H. Luo, Y. Wu, J. W. Fu, Q. G. He, J. G. Cheng, J. Na, Y. Yamauchi and S. H. Liu, *J. Mater. Chem. A*, 2021, **9**, 8308–8316.
76 M. Setka, R. Calavia, L. Vojkuvka, E. Llobet, J. Drbohlavova and S. Vallejos, *Sci. Rep.*, 2019, **9**, 8465.
77 J. Cao, H. M. Dou, H. Zhang, H. X. Mei, S. Liu, T. Fei, R. Wang, L. J. Wang and T. Zhang, *Sens. Actuators, B*, 2014, **198**, 180–187.
78 Y. G. Wang, L. C. Yao, L. J. Xu, W. H. Wu, W. H. Lin, C. H. Zheng, Y. Q. Feng and X. Gao, *Sens. Actuators, B*, 2021, **332**, 129497.
79 T. T. Nguyet, C. M. Hung, D. T. T. Le, N. V. Duy, N. D. Hoa, F. Biasioli, M. Tonezzer and C. Di Natale, *Ceram. Int.*, 2021, **47**, 28811–28820.
80 J. Li, Y. J. Lu, Q. Ye, M. Cinke, J. Han and M. Meyyappan, *Nano Lett.*, 2003, **3**, 929–933.
81 M. Das and S. Roy, *Mater. Sci. Semicond. Process.*, 2021, **121**, 105332.

82 S. Bibi, H. Ullah, S. M. Ahmad, A.-u.-H. A. Shah, S. Bilal, A. A. Tahir and K. Ayub, *J. Phys. Chem. C*, 2015, **119**, 15994–16003.
83 A. R. Baggio, D. F. S. Machado, V. H. Carvalho-Silva, L. G. Paterno and H. C. B. de Oliveira, *Phys. Chem. Chem. Phys.*, 2017, **19**, 10843–10853.
84 S. Aarya, Y. Kumar and R. K. Chahota, *J. Inorg. Organomet. Polym. Mater.*, 2020, **30**, 269–290.
85 Y. X. Qin, B. Y. Zhang and Z. Zhang, *Org. Electron.*, 2019, **70**, 240–245.
86 S. J. Gai, B. Wang, X. L. Wang, R. Z. Zhang, S. L. Miao and Y. Q. Wu, *Sens. Actuators, B*, 2022, **357**, 131352.
87 G. Zamiri and A. Haseeb, *Materials*, 2020, **13**, 3311.
88 C. K. She, G. S. Li, W. Q. Zhang, G. X. Xie, Y. Zhang, L. Li, F. Y. Yue, S. H. Liu, C. B. Jing, Y. Cheng and J. H. Chu, *Sens. Actuators, A*, 2021, **317**, 112436.
89 D. Caballero, L. Fumagalli, F. Teixidor, J. Samitier and A. Errachid, *Sens. Actuators, B*, 2013, **177**, 1003–1009.